Icarus 408 (2024) 115853

Contents lists available at ScienceDirect

Icarus

journal homepage: www.elsevier.com/locate/icarus

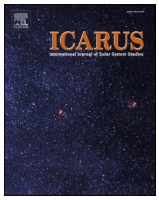

Petrogenesis of magnesian troctolitic granulite clasts from Chang'e -5 drilling sample: Implications for the origin of ejecta material from lunar highlands

Qi He [a,*], Zhi Cao [a,b], Yuqi Qian [c], Hejiu Hui [d], Ioannis Baziotis [e], Long Xiao [a], Zaicong Wang [a], Biji Luo [a], Yiheng Li [a], Zongjun Ying [f], Yang Li [b]

[a] Planetary Science Institute, State Key Laboratory of Geological Processes and Mineral Resources, School of Earth Sciences, China University of Geosciences, Wuhan 430074, China
[b] Center for Lunar and Planetary Sciences, Institute of Geochemistry, Chinese Academy of Sciences, Guiyang, China
[c] Department of Earth Sciences, The University of Hong Kong, Hong Kong, China
[d] School of Earth Sciences and Engineering, Nanjing University, Nanjing 210023, China
[e] Department of Natural Resources Management & Agricultural Engineering, Agricultural University of Athens, Iera Odos 75, Athens 11855, Athens, Greece
[f] State Key Laboratory of Palaeobiology and Stratigraphy, Nanjing Institute of Geology and Paleontology & Center for Excellence in Life and Paleoenvironment, Chinese Academy of Sciences, Nanjing 210008, China

ARTICLE INFO

Keywords:
Lunar soil
Mg-suite
Granulite
Moon
Petrogenesis

ABSTRACT

The lunar soil collected by the Chang'e-5 (CE-5) mission contains both local materials and components of various sources. The latter could have derived from the excavation of impact craters in the highlands away from the landing site, providing valuable information on the composition of the lunar crust beyond the mare basalts sampled by the CE-5 mission. In this study, we examined the mineralogy and petrology of magnesian troctolitic granulites (or troctolites) recovered in the CE-5 soil. The troctolites exhibit a granoblastic texture but have a finer grain size compared to Apollo granulites, and almost all plagioclase remains unaltered and not converted to maskelynite. The major element composition shows a SiO_2 content of 45.4 wt%, CaO of 12 wt%, TiO_2 of 0.2 wt%, Th of 0.1 ppm, and an Mg# of 76, lower than those of the Mg troctolitic lunar meteorites NWA 5744 and NWA 10401. The trace element budget indicates that the magnesian troctolites are KREEP-poor, which distinguishes them from the Mg-suite rocks in Apollo samples but is similar to some troctolitic lunar meteorites (NWA 10401). Furthermore, we predict –by using MELTS modeling– a plausible genetic connection between the Mg-suite rocks, and our troctolites, suggesting that the latter may be pristine and formed during a later stage along a fractional crystallization path. This scenario challenges the hybridization model and strengthens the evidence in favour of the fractional crystallization modeling. To ascertain the potential origin crater for the magnesian granulites, a comparative analysis was conducted with NWA 10401. Based on our findings, we propose that the Pythagoras crater, situated north of the CE-5 landing site, is the most probable source of the aforementioned magnesian troctolitic granulites. The ejecta from this crater may have been deposited between the Eratosthenian-aged mare basalts and the Imbrian-aged mare basalts beneath the CE-5 landing site. The KREEP-poor troctolitic granulite in the Chang'e-5 soil could represent paleo-ejecta from Pythagoras crater, excavated by subsequent impacts on the Eratosthenian-aged basalts and delivered them to the CE-5 site. The original location of the Mg troctolitic granulites is inferred to be near-surface, buried by the uppermost crustal rocks (<10 km), which is consistent with its contact with feldspathic impact glass.

1. Introduction

The ancient lunar crust contains valuable information on the magmatic differentiation processes that occurred during the early history of the Moon (Shearer et al., 2006). Non-mare igneous rocks, such as ferroan anorthosite (FAN) and magnesian suite (Mg-suite), are particularly important (Papike et al., 1998; Wieczorek et al., 2006). FANs are suggested to represent the primary crust, originating directly

* Corresponding author.
E-mail address: he_qi@cug.edu.cn (Q. He).

https://doi.org/10.1016/j.icarus.2023.115853
Received 13 April 2023; Received in revised form 7 October 2023; Accepted 30 October 2023
Available online 5 November 2023

from the global magma ocean and comprising the majority (~80%) of the lunar highlands (Dowty et al., 1974; Wieczorek et al., 2006). Mg-suite rocks, on the other hand, are Mg-rich plutonic rocks that likely originated from the lower lunar crust with few outcrops exposed on the lunar surface (McCallum and Schwartz, 2001). The Mg-rich rocks account for only a small proportion of lunar samples (around 0.7% of the 381.7 kg of samples returned by the Apollo programs)(Wieczorek et al., 2006). Early studieson the Apollo samples suggested that Mg-suite magmatism was strongly influenced by KREEPy magma and was closely associated with the Procellarum KREEP Terrain (PKT)(Shearer and Papike, 2005; Shearer et al., 2006). However, recent –trace element– studies on lunar meteorites (Gross et al., 2020; Takeda et al., 2006; Treiman et al., 2010) and geochemical models (Prissel et al., 2014; Prissel and Gross, 2020), indicate that high-magnesium rocks can also be crystallized from KREEP-poor melts, suggesting that the distribution of Mg-suite rocks could be lunar-wide.

Previous studies on ejecting material from impact crater (Qian et al., 2021a) and CE-5 soils (Li et al., 2022) have shown that the Chang'e-5 (CE-5) samples mainly comprise weathering products of local basaltic materials with a small amount of materials (<10%) originating from distal craters. However, non-local materials in the CE-5 soils may be more representative of the lunar crust since impact cratering can bring various materials to the landing site. Raman spectroscopy has revealed that the small amount of non-local materials in CE-5 soils (5–7%) are mainly Mg-suite rocks (Mg # >70; Cao et al., 2022), while several calcic plagioclases and clasts likely originate from the ancient Feldspathic Highland Terrane (FHT; Li et al., 2022; Sheng et al., 2022). Additionally, seifertite and stishovite, possibly distant ejecta from the Aristarchus crater to the CE-5 site, have been found (Pang et al., 2022). Recently, Zeng et al. (2023) also identified 7 igneous clasts in the CE-5 samples from >3000 regolith particles (surface scoop sample). These materials provide an opportunity to learn more about the complex evolutionary history of the lunar crust.

In the present study, we have discovered two magnesian troctolitic granulite clasts within the CE-5 soil samples. The mineralogical and chemical data of these fragments have been provided, and we have undertaken a comparative analysis with Mg troctolitic granulites found in lunar meteorites. The objective of this study is to establish constraints on the origin and formation of these granulites, as well as to ascertain any potential connections with a KREEP-poor Mg-suite parental melt. The discovery of these KREEP-poor Mg troctolitic granulites in CE-5 samples has significant implications for understanding the early lunar crustal formation and evolution, as well as the early history of the Moon.

2. Samples and analytical methods

A 150 mg aliquot (CE5Z0204YJFM002) CE-5 drilling sample was allocated by the China National Space Administration for this study. Large lithic clasts (typically >70 μm) were manually picked from the aliquot. Two have been used for the current study (HQ002,12 and HQ1–9), with a total mass slightly lower than 1 mg. The lithic clasts were mounted in Araldite 2020 epoxy resin and polished for petrographic observations.

Polished mounts were carbon-coated and examined with the scanning electron microscope (SEM, FEI Quanta 200) equipped with energy dispersive spectrometers (EDS) at the State Key Laboratory of Geological Processes and Mineral Resources, China University of Geosciences, Wuhan (GPMR-CUG). Thick sections were examined for back-scattered electron (BSE) imaging and X-ray elemental mapping.

Major element compositions of minerals were determined using a JEOL JXA-8230 electron microprobe analyzer (EPMA) at GPMR-CUG. Minerals were analyzed using a 15 kV acceleration voltage and a 20 nA focused beam typically at 3 μm diameter for silicates. For silicate and oxide phases, the standards used for ZAF matrix correction were jadeite (Na), olivine (Si), diopside (Ca, Mg), almandine (Fe, Al), sanidine (K), rutile (Ti), rhodonite (Mn), and chromium oxide (Cr). Furthermore, Na and K were analyzed first to avoid volatile loss. Representative EPMA results are given in Table S1, while the detailed compositions are given in the Tables S2–1, S2–2, S2–3, and S2–4.

Major and trace element contents of minerals or clasts were obtained from the polished mounts using laser ablation inductively coupled plasma mass spectrometry (LA-ICP-MS). Trace element analyses were obtained using an Agilent 7500a ICP-MS coupled with a Geolas Shearer and Papike, 2005 excimer ArF laser (193 nm) ablation system (Lambda Physik, Göttingen, Germany). The repetition rate used was between 6 and 10 Hz. Additionally, incorporating nitrogen into the gas flow helped to increase the detection limit and improve precision (Hu et al., 2008). Each analysis included a background acquisition of 20–30 s (gas blank) followed by 50 s of sample data acquisition. The software ICPMSDataCal was used for off-line selection and integration of the background and analyzed areas, time-drift correction, and data reduction (Liu et al., 2008).

The small sizes of the olivine, pyroxene, and chromite grains in HQ002,12 are unsuitable for LA-ICPMS analysis. The spot diameter used for plagioclase was 32 μm, while that used for fine-grained clasts was 90 μm. The clasts –made of multiple minerals– were analyzed simultaneously in one run, using line scan mode. The measured elements were calibrated externally using several USGS glasses (BCR-2G, BHVO-2G, and BIR-1G) with preferred values for USGS glasses obtained from the Geological and Environmental Reference Materials-GeoReM database (http://georem.mpch-mainz.gwdg.de; Jochum et al., 2005). In order to achieve sufficient standardization, a measurement of NIST SRM 610 glass was conducted after every six unknown measurements. Major and trace element results obtained through LA-ICP-MS are presented in Table S3. More details on standard analyses are provided in Table S4.

We have determined the modal abundances of plagioclase, olivine, orthopyroxene, clinopyroxene, and chromite within the HQ002,12 sample. The selection of the analytical region for X-ray mapping was based on the inclusion of both the Mg-troctolitic granulite The X-ray maps acquired using the SEM instrument for specific elements (Si, Al, Ca, Mg, Fe, and Cr), and subsequently were imported as raw files into ImageJ software. The mode of each mineral was then estimated by counting the pixels associated with a particular color of each mineral within the HQ002,12. Two distinct methods were employed to estimate the bulk-rock major element composition. The first approach involved combining the measured average mineral chemistry of plagioclase, olivine, pyroxene, and Ti-chromite with the modal content of each mineral. The second approach employed broad line scan mode ablations of LA-ICP-MS in three different regions of the fine-grained matrix. It is important to note that the reconstructed bulk composition of the small clast may not be entirely representative due to measurement or calculation discrepancies. Additionally, the uncertainty associated with the abundance of elements present in rare mineral grains (such as P in phosphate and Ti in ilmenite) is difficult to quantify.

3. Results

3.1. Petrography and mineral chemistry

Two magnesian troctolitic granulite clasts have been identified in our samples (HQ002,12 and HQ1–9), and we focus on HQ002,12 in this study. HQ002,12 is a composite clast consisting of two distinct lithologies (Fig. 1). The first lithology corresponds to anorthosite (approximate size 350 × 100 μm), consisting of a large plagioclase crystal (140 × 70 μm) and feldspathic impact glass. The second lithology is a magnesian troctolitic granulite which is cross-cut by feldspathic-glass (Fig. 2c). The large plagioclase within the first lithology is rich in anorthite component ($An_{95.7–97.7}$; An = Ca/[Ca + Na + K] × 100). The magnesian troctolitic granulite is approximately 200 × 400 μm in size showing a granoblastic texture (Fig. 2d). The troctolitic granulite consists of plagioclase (64.6 vol%), olivine (23.7 vol%), orthopyroxene (8.4 vol%), clinopyroxene (3.2 vol%), and traces of chromite and troilite (<0.1 vol

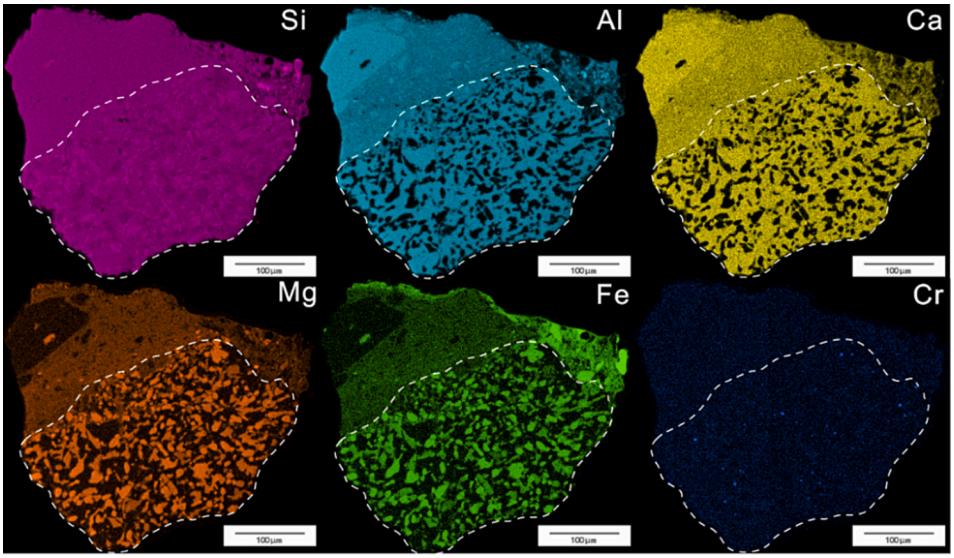

Fig. 1. X-ray maps of the HQ002,12, the white dot line circle the Mg troctolitic granulites.

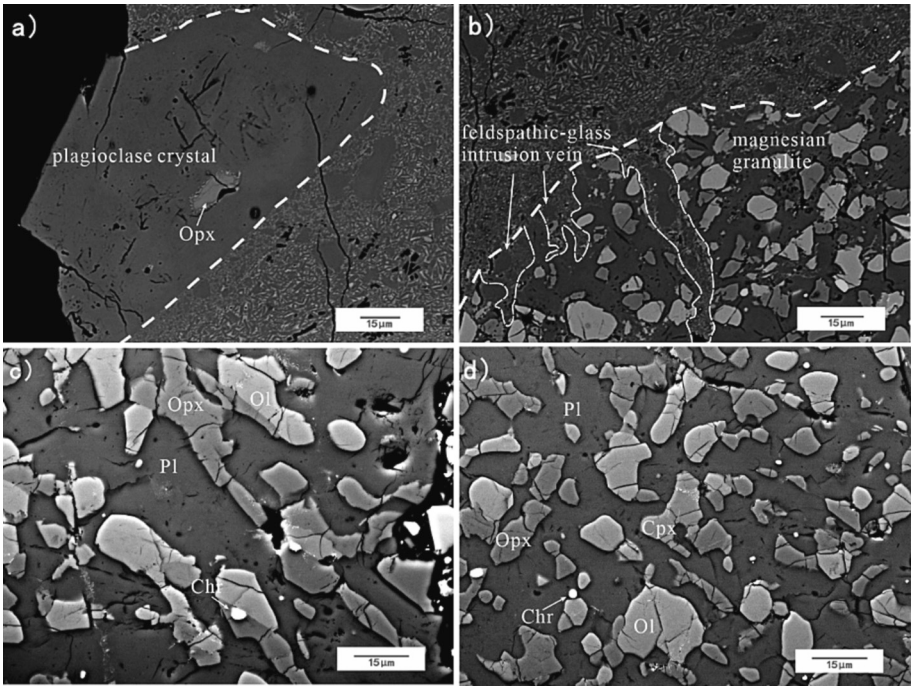

Fig. 2. BSE images of HQ002,12. a) The anorthosite component is consisted of one large plagioclase crystal and feldspathic impact glass. b) Feldspathic-glass intrusion veins of magnesian granulite at the boundary between feldspathic impact glass and magnesian granulite. c, d) Granoblastic texture of magnesian granulite composed by irregularly shaped –anhedral to subhedral– grains of olivine, orthopyroxene and clinopyroxene embedded and intergranular plagioclase.

%)(Table 1). Following theclassification criteria in Stöffler et al. (1980), this cast could be regarded as an anorthositic troctolite.

The individual subhedral to anhedral olivine and pyroxene grains (5–25 μm) are roughly equant, and occurred in coarse-grained plagioclase dominated matrix. Most plagioclases –especially those with a size ~40–70 μm in width– display rounded edges. Many of these plagioclase grains are poikilitic and enclose small olivine grains (< 5 μm in diameter) that tend to occur near the rims. Some relict igneous textures have been observed (Fig. 2) as indicated by the presence of subhedral relics of euhedral plagioclase laths. Some olivine grains are partially surrounded by orthopyroxene, suggesting the crystallized reaction olivine + melt → orthopyroxene (e.g., (Morse, 1980).

The mineral grains are chemically homogeneous. The olivine is highly forsteritic $Fo_{74.7–76.5}$ (Table S1), being slightly lower than the respective reported for Mg granulites NWA 5744 ($Fo_{78.0–82.1}$) and NWA 10401 ($Fo_{79.2–84.3}$) (Kent et al., 2017; Gross et al., 2020), but higher than that of Fe granulites like NWA 3163 ($Fo_{57.9}$)(Hudgins et al., 2011). Orthopyroxenes have composition of $En_{76.5–77.7}Fs_{19.2–19.8}Wo_{2.9–4.1}$; clinopyroxenes have composition of $En_{48.3–50.2}Fs_{8.6–10.9}Wo_{38.9–42.2}$. Both pyroxenes have almost similar composition with pyroxenes from other Mg granulites such as NWA 10401 (Fig. 3; Gross et al., 2020). The Mg# in pyroxenes ranges from 79.5 to 85.2, with an average Mg# of 81.4. Plagioclase matrix grains have a compositional range of $An_{94.1–97.9}$ (Table S1).

Pyroxene chemistries could have been altered by metamorphism, but they may still retain some primary crystallization signatures. (Bence and

Table 1
The Bulk Modal Mineralogy for Magnesian Granulitic in HQ002,12 Compared to Mineral Modes of NWA 10401 and NWA 5744.

Mineral(vol %)	HQ002,12		NWA10401	NWA 5744
	Modal mineralogy	Mass proportion		
Pl	64.6	59.4	67	59–65
Ol	23.7	27.8	26.3	23–26
Opx	8.4	8.9	6.3	12–15*
Cpx	3.2	3.7	0.3	
Chr/Spinel	0.1	0.2	0.1	–

* incudes Opx and Cpx. NWA 10401 data from Gross et al. (2020); NWA 5744 data from Kent et al. (2017).

Papike, 1972; Day et al., 2006). The orthopyroxenes on the Al^{VI}-Cr-Ti plot define a trend from a high Al^{VI} content to a composition enriched in Ti (Fig. 4a). Further, the titanium-aluminum relationships indicate a slight decrease of Ti/Al, and them constant increase of Ti with Al (Fig. 4b). This is in accordance with the formation of Ca-free orthopyroxene, and then progressively evolves towards Fe-richer orthopyroxenes with increase Si/Al ratios (Fig. 4c). These orthopyroxene compositional trends (Fig. 4) are consistent with continues crystallization before the onset of pigeonite/augite formation. The clinopyroxenes reveal a composition mainly of augite. The EPMA analyses define a high-Al^{VI} core, and moving towards Ti-rich pyroxene in the Al^{VI}-Cr-Ti plot (Fig. 4a). This correlates with the low Ti/Al (1/4) and high Al/Si ratios recorded on the early clinopyroxene suggesting crystallization from a liquid saturated in Al.

Accessory phases are mainly represented by the spinel-group minerals. Spinel-group minerals such as Ti-chromite are usually very small in size (1-3 μm) and occur within plagioclase or associated with olivine grains. The Ti-chromites have a composition of $Chr_{61.2–70.0}Sp_{20.1–24.2}Ulv_{6.6–16.7}$ displaying variable amounts of Al_2O_3 (9.66–11.9 wt%), TiO_2 (2.54–6.45 wt%), Cr_2O_3 (45.1–50.4 wt%), and FeO (27.7–30.7 wt%) (Tables S1, S2–4).

HQ1–9 is also a Mg troctolitic granulite. It is approximately 600 × 400 μm in size. It has poikilitic texture (Fig.S1, S2, supplementary video 1). The granulite is consisted of plagioclase (62.2 vol%), olivine (20.4 vol%), pigeonite (12.1 vol%), minor amount of ilmenite (3.5 vol%), and traces of troilite and Fe—Ni metal (1.8 vol%)) (in vol%, estimated by ImageJ software). Additionally, a single, 5 μm long, zircon grain has been found associated with ilmenite.

Unlike HQ002,12, almost all the plagioclases in the HQ1–9 are maskelynite. The maskelynite is rare in CE-5 sample but is commonly observed in lunar meteorites, which imply relatively high shock level (Cao et al., 2022).

3.2. Bulk composition and trace element composition of plagioclase

Three different ablation measurements are consistent with each other (Table S3). The clast's mean bulk composition has SiO_2, CaO, TiO_2, and Th of 45.4 wt%, 12.0 wt%, 0.2 wt%, and 0.1 ppm, respectively. The Mg# of the clast HQ002,12 is 76, which is lower than of NWA 5744 (79–80; Kent et al., 2017; Korotev and Irving, 2016) and NWA 10401 (82, the highest Mg# of known feldspathic meteorite samples so far; Gross et al., 2020).

The REE pattern of HQ002,12 is similar to that of NWA 5744, and NWA 10401. Both are flat for LREE and HREE with a positive Eu anomaly. Meanwhile, the REE pattern of HQ002,12 is most similar to that of NWA 5744, and that NWA 10401 is even poorer in KREEP. The bulk trace element content of HQ002,12 shows very low incompatible element abundance, i.e., negligible KREEP content (KREEP-poor) (Fig. 5). If this clast is representative of the protolith(s), it is most likely that HQ002,12 originated from FHT that is different from Apollo landing sites.

Plagioclase is enriched in light rare earth elements (LREE) relative to heavy rare earth elements (HREE) (CI-normalized La/Yb ratio of 17.9, Fig. 5) and contains positive Eu anomalies, typical of lunar highland rocks.

4. Discussion

4.1. Comparison with other granulites

The clast HQ002,12 is a non-local material. The calcic plagioclases cannot be from the CE-5 basalts because the plagioclase for CE-5 basalts has a composition of $An_{68–90}$ (He et al., 2022; Tian et al., 2021), but most likely originating from FHT (Stoffler, 2006). The clast HQ002,12 is

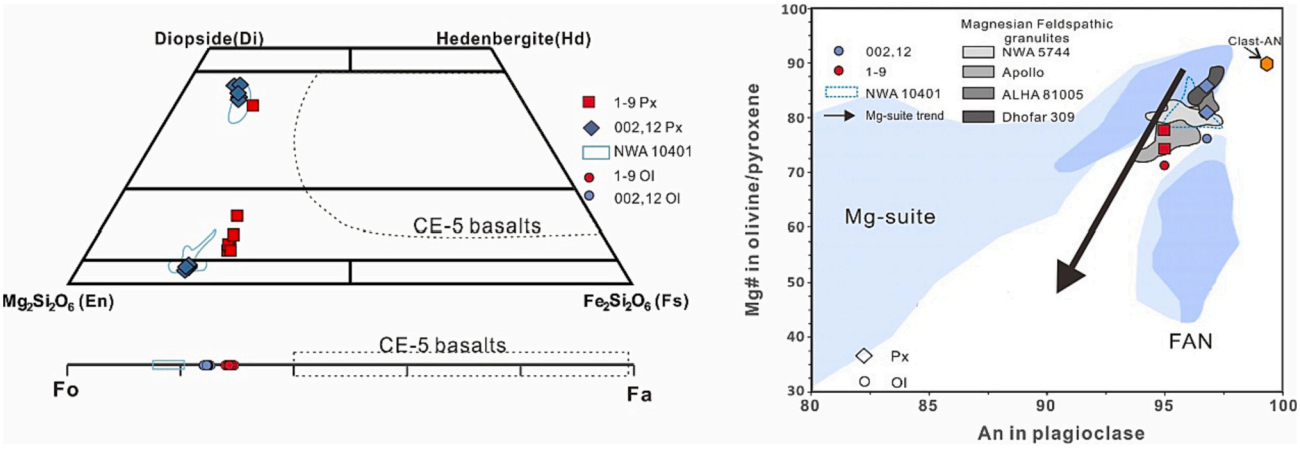

Fig. 3. Comparison of mineral chemistry in magnesian granulitic domain of HQ002,12, in relation to the meteoritic granulite NWA 10401. (a) Pyroxene (upper) and olivine (lower) mineral composition; (b) The An# [molar Ca/(Ca + Na + K)] in plagioclase is plotted versus Mg# [molar Mg/(Mg + Fe)] for mafic minerals (pyroxene and olivine) present in HQ002,12. Clast-AN is the Mg-suite clast recognized in Chang'e-5 regolith by Zeng et al. (2023). The field for Chang'e-5 basalts are after Tian et al. (2021) and He et al. (2022). The shaded fields for Mg-suite and FAN are after (Yamaguchi et al., 2010), which represent fields for lunar pristine rock suites (FAN and Mg-suite) from the Apollo missions and indicate the pristinity index of (Warren, 1993). Light grey region is based on individual EMP measurements of NWA 5744 olivine grains versus plagioclase matrix, physically located within 25 μm of each other (Kent et al. (2017). Magnesian feldspathic granulites data for ALHA 81005 and Dhofar 309 are based on Goodrich et al. (1984) and Treiman et al. (2010). The Apollo magnesian feldspathic granulites data are from samples 60,035, 67,415, 67,955, 72,275, 76,230, and 79,215 (Ma and Schmitt, 1982; Lindstrom and Lindstrom, 1986; Salpas et al., 1988). The black arrow corresponds to Mg-suite crystallization trend (KREEP-free) given in Fig. 7 of Prissel and Gross (2020).

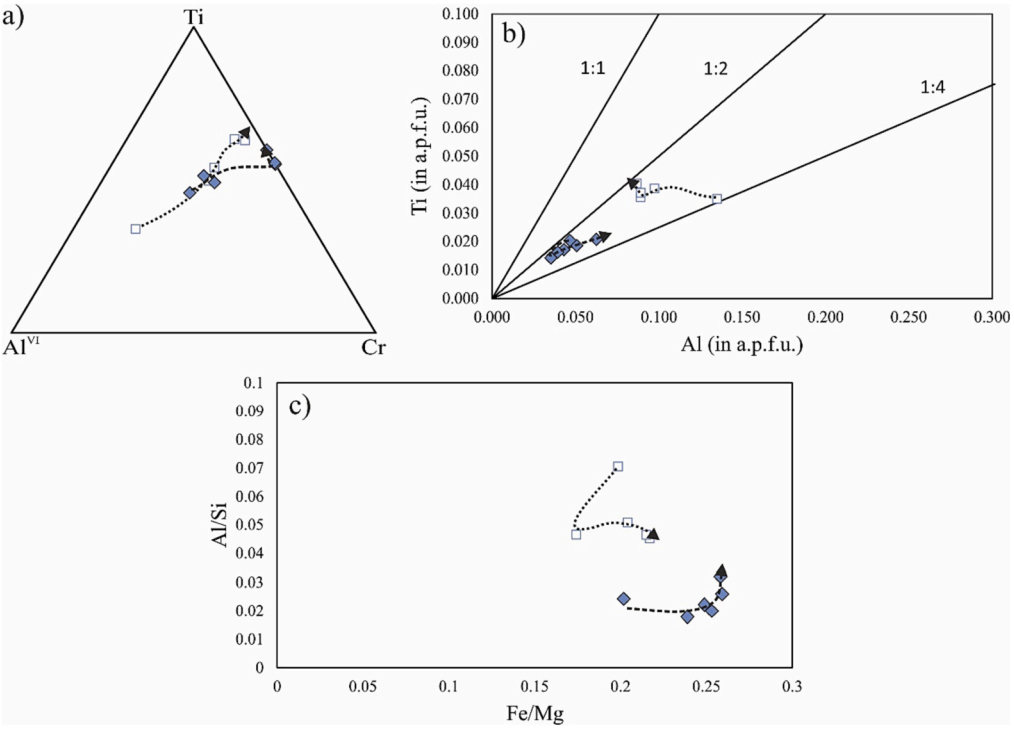

Fig. 4. Pyroxene chemistry for the studied clasts in HQ002,12 as a function of Al^{VI}-Cr-Ti (plot a), Ti vs Al (in atoms per formula unit-a.p.f.u.)(plot b), and Al/Si vs Fe/Mg (plot c). The measured pyroxenes within the HQ002,12 follow the recognizing crystallization sequences defined in Bence and Papike (1972). The dashed and dotted lines correspond to the compositional trends for orthopyroxene and clinopyroxene, respectively. Lines in b) denoted 1:1, 1:2, 1:4 indicate ratios of Ti/Al = 1.0, 0.5, and 0.25, respectively.

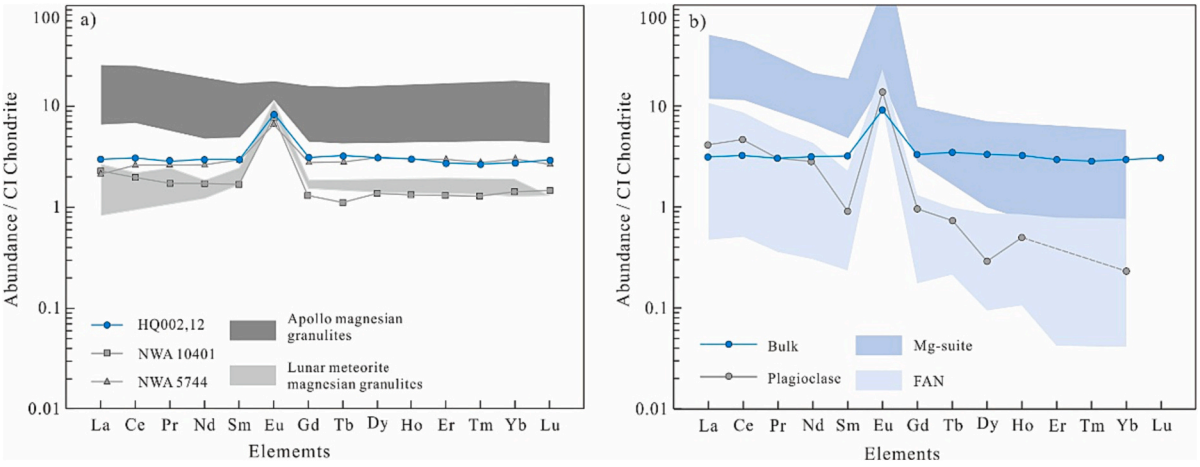

Fig. 5. CI chondrite normalized REE values of bulk rock and plagioclase in Mg granulites in HQ002,12. REE abundance of CI chondrite were (McDonough and Sun, 1995). (a) REE distribution pattern of bulk sample compared to Apollo FAN, Mg-suite, and anorthositic granulites in meteorites NWA 5744 and NWA 10401(Kent et al., 2017; Gross et al., 2020). Light shaded area represents REE abundance of Dhofar 489 (Takeda et al., 2006), ALH 81005 (Treiman et al., 2010) and Dhofar 309 (Treiman et al., 2010). Dark shaded area represents REE abundance of 60,035 (Ma and Schmitt, 1982; Hudgins et al., 2008), 72,275 (Salpas et al., 1988), 76,503 and 72,503 (Jolliff et al., 1996), 79,215 (Hudgins et al., 2008); (b) REE distribution pattern of plagioclase in NWA 10401 compared to Apollo FAN, Mg-suite, and anorthositic granulites in meteorites. Light shaded area represents data from Papike et al. (1997); Floss et al. (1998). Dark area shows data from Papike et al. (1996); Shervais and McGee (1998).

primarily composed of a metamorphic matrix, composed of relatively fine-grained (<30 μm in width) olivines and pyroxenes surrounded by plagioclase (Fig. 2). The texture for HQ002,12 is similar to Apollo granulitic breccia samples such as 60,035, 77,017, 78,155, and 79,215 (Hudgins et al., 2008). The texture is also similar to granulites in lunar meteorites, such as ALHA 81005, Dar Al Gani 400, Dhofar 025, NWA 3163, ALH 81005, Dhofar 309, NWA 5744, NWA 10401, MacAlpine Hills 88,105 and Shişr 161 (Hudgins et al., 2011; Treiman et al., 2010; Korotev, 2012; Kent et al., 2017; Joy et al., 2010; Gross et al., 2014, 2020), ranging from poikiloblastic to granoblastic (Hudgins et al., 2011). However, the grain sizes in lunar meteorites are much coarser than that in HQ002,12, which has a typical mafic mineral grain size of 0.1–0.2 mm. Based on the work of Bickel and Warner (1978), the granulites can be subdivided into different grain size groups (fine <100 μm, medium 100–200 μm and coarse >200 μm). Therefore, the HQ002,12 could be a fine-grained troctolitic granulite. Because the

small grain size, the pyroxene exsolution was not observed in the CE-5 samples but in some samples with large sized pyroxenes with 1–5 μm thick lamellae (Gross et al., 2020).

Another difference between HQ 002,12 and lunar meteorites (granulites and other compositions) is that almost all of the plagioclase in the meteorites has been converted to maskelynite (Treiman et al., 2010; Kent et al., 2017); Gross et al., 2020), while the plagioclase in HQ002,12 is still crystalline. Only few grains were converted to maskelynite at the edge of the clasts. Furthermore, the presence of irregular fractures within olivines indicate that the rock has shocked at stage up to S3 (Stöffler et al., 2018). Glassy and microcrystal FAN contact with the Mg troctolitic granulite in HQ002,12, reflecting the injection of impact melt within pre-existing shock-induced fractures.

On the basis of the Apollo samples, (Lindstrom and Lindstrom, 1986) advocated that granulitic breccias were dichotomous, with ferroan [Mg# = Mg/(Mg + Fe) <65] and magnesian (Mg# >72) groups. It is notable that lunar meteorites also contain two sub-types: (1) a ferroan sub-type including NWA 3163 (and pairs NWA 4881/4483) (McLeod et al., 2016) and Dho 026, and (2) a Mg-rich sub-type, namely the Magnesian granulites including NWA 5744 and its pairs (at least six include NWA 8687, NWA 10401) and the Dhofar 303 clan (Treiman et al., 2010; Korotev and Irving, 2016); (Kent et al., 2017). The clast HQ002,12 from this study is similar to the Mg-rich sub-type, thus referred here as "Mg troctolitic granulite".

The Ni concentration in the bulk exhibits a low range of 75–128 ppm, whereas the bulk ratio of Ni/Co ranges from 3.63 to 5.37, approximating a value of 5. This ratio is consistent with that observed in other granulitic breccias found in meteorites (Hudgins et al., 2008). As noted by (Haskin et al., 1998), granulitic breccias from Apollo 17 are rich in siderophile elements. These elements are carried by Fe —Ni metal grains, such as those in (Hudgins et al., 2008) for samples 77,017, 78,155, and 79,215. Metal grains in HQ002,12 are rare and bulk rock concentrations of Ni are consequently much lower than in the Apollo 17 samples, which show limited contamination by meteorites and therefore representing the original lunar composition.

The Al_2O_3 component of the bulk rock vs. Mg# (Fig. 6) indicates that mixing of typical feldspathic FAN with a potential mantle component (peridotite) would result in a rock type that would have the same Al_2O_3 and Mg# composition than HQ002,12 like the NWA 5744 and NWA 10401. Thus, it is possible that the protolith of HQ002,12 also could represent a mixture of FAN and KREEP-poor Mg-rich mantle material (Gross et al., 2020). The KREEP-poor nature of HQ002,12 precludes the involvement of the KREEP-bearing Apollo Mg-suite lithologies as a protolith. HQ002,12 has lower Mg# compare with NWA 5744 and NWA 10401. This is also consistent with the proposal that mantle-derived melt as heat and material source, which have melted the primordial anorthosites and mixed to form the Mg-suite magma (Xu et al., 2020) or the hybridization melting model proposed by Shearer et al. (2015). However, the mixing of Mg-rich component (peridotite) and anorthositic crust should lead to low-Cr and high-Al spinel rock types (Pieters et al., 2014; Prissel et al., 2016a, 2016b), which is different from the observation in this study.

On the other hand, Prissel and Gross (2020) proposed that the Mg-suite primary melt was mantle-derived (via decompression melting of a peridotite mantle) to either crystallize KREEP-free lithologies (such as those observed here), and/or had secondary interactions with crustal or KREEPy material to explain the minor abundance of spinel-bearing troctolites or REE-elevated samples. Meanwhile, Pieters et al., 2014; Prissel et al., 2016a, 2016b) experimentally show that partial melts from Mg-rich cumulate + FAN crust sources consistently yield low-Cr and high-Al spinel. This result is in conflict since chromite-bearing troctolites are the norm and low-Cr high- Al spinel-bearing troctolites are volumetrically minor (< 2% of all lunar troctolites by mass; Prissel and Gross, 2020). Chromite is ubiquitous among many olivine-normative and mantle-derived melts. The presence of chromite (not spinel) in the clast appears to support derivation from a more typical peridotitic

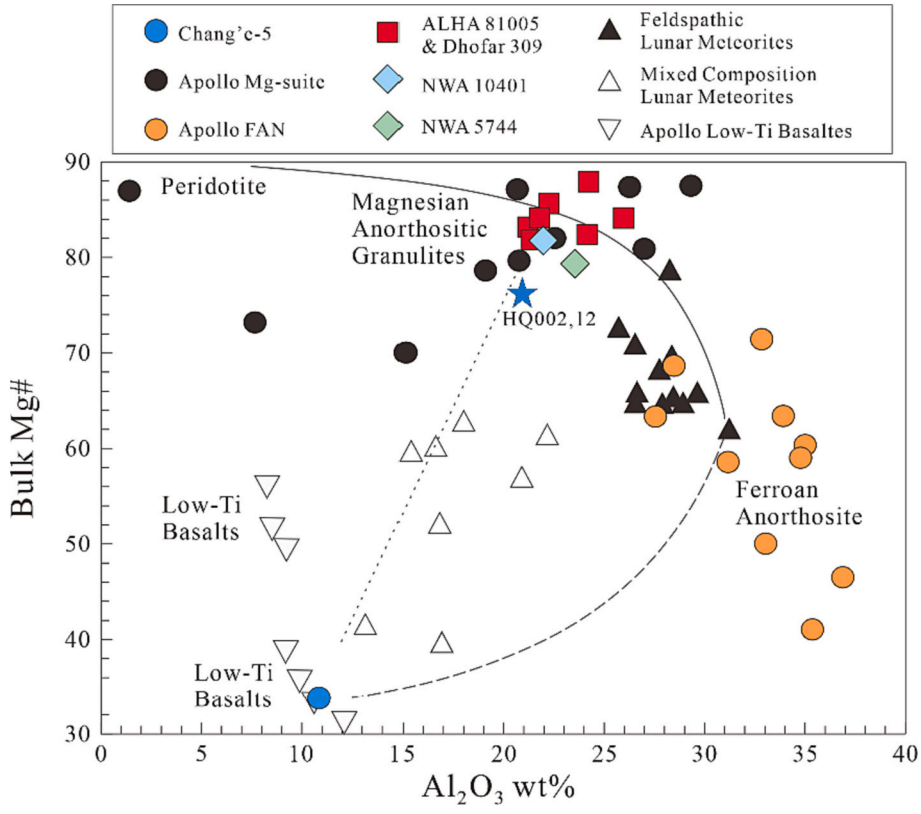

Fig. 6. Bulk-rock Al_2O_3 contents versus Mg#. Mixing of typical FAN with a potential mantle component (peridotite) could result in a rock type with Al_2O_3 and Mg# compositions similar to HQ002,12. It is possible that the protolith of HQ002,12 could represent a mixture of FAN and KREEP-poor and Mg- rich mantle material.

source such as the partial melts modeled in Prissel and Gross (2020).

As modeled in Prissel and Gross (2020), mantle-derived melts can evolve to plagioclase saturation during fractional crystallization, producing a similar trend of decreasing Mg# and increased Al_2O_3 as shown in Fig. 6 but importantly requires no mixing between peridotite and anorthosite.

The Mg-suite rocks are characterized by high Mg# and low Cr_2O_3 contents. In our study, the clast HQ002,12, hosts olivines with low Cr_2O_3 contents (100–800 ppm, Table S1) at relatively intermediate Fo content (range between 74.7 and 76.5). This Cr_2O_3 content is significantly lower than the estimate from the fractional crystallization produced from the early LMO cumulates (1900–3800 pppm, Elardo et al., 2011, Fig. 7), while the Fo is intermediate between the early magma ocean cumulates (range from 88.9 to 95.6, Elardo et al., 2011), the Mg-suite and the Mare basalts. Furthermore, the thermodynamic modeling work by Ju et al. (2021) considered the chromite as the residual solid phase and suggested that the Mg-suite could be formed by the equilibrium crystallization of the melt derived from the decompression melting of the lunar mantle materials, with its olivine containing low Cr_2O_3 content (Fig. 7). Furthermore, the presence of chromite becomes important for distinguishing between fractional crystallization of mantle-derived melts (Prissel and Gross, 2020) versus anorthosite mixing: chromite suggests that the parental melt was plagioclase-undersaturated, meaning it was a more typical olivine-normative mantle-derived melt and not a hybridized melt with initially high-Al contents from plagioclase mixing.

Moreover, in the equilibrium crystallization model proposed by Ju et al. (2021), the chromium (Cr) content of olivine exhibits a variation along the early fractionation segment, ranging from Fo_{95} to Fo_{90}, before rapidly decreasing due to the co-crystallization of Cr-rich spinel. Consequently, if all the Cr is moving out of the system, while Al is accumulating, the composition of spinel is expected to shift from chromite towards spinel. Thus, Cr becomes less compatible in the entire fractionating assemblage and might appear relatively constant (approximately) on a plot such as Fo vs Cr_2O_3 content (Fig. 7) as the olivine continues to evolve.

This phenomenon has been explored here for both equilibrium and fractional crystallization models. We utilized the easyMELTS interface to the MELTS model (http://magmasource.caltech.edu) to track the major and trace elements (Ghiorso and Sack, 1995; Asimow and Ghiorso, 1998; Asimow, 1999; Asimow et al., 2001; Asimow et al., 2004; Smith and Asimow, 2005).

In this approach, we examined the magmatic evolution from the most primitive (lower SiO_2/highest MgO) analysis obtained from the literature (melt B-1; Table 2 in Ju et al., 2021), assessing whether its liquid line of descent passes through the more evolved olivine compositions (towards lower Fo content). It's crucial to note that the MELTS model for olivine (and any version of MELTS) does not include Cr. The only solid phase that hosts Cr in the MELTS models is spinel. Therefore, we retrieved partition coefficient data from the literature and used only those experiments that contain both olivine and liquid with measured Cr_2O_3 content.

In our MELTS model, the Cr behavior is solely controlled by how much is extracted through Cr-spinel fractionation, influencing changes in the Cr content of the liquid. We then determined the Cr content in coexisting olivine using partition coefficients published by Longhi et al. (1978). These experiments were conducted at varying temperatures (1375, 1328, 1300, 1249, 1216, 1201, 1175, 1158, 1156, 1133 and 1124 °C). We plotted these temperatures against the respective partition coefficient values, revealing a strong correlation ($r = 0.8$), and we derived a polynomial equation of the form: $DCr^{Ol}_{melt} = 2 \times 10^{-5} \times T^2$ -

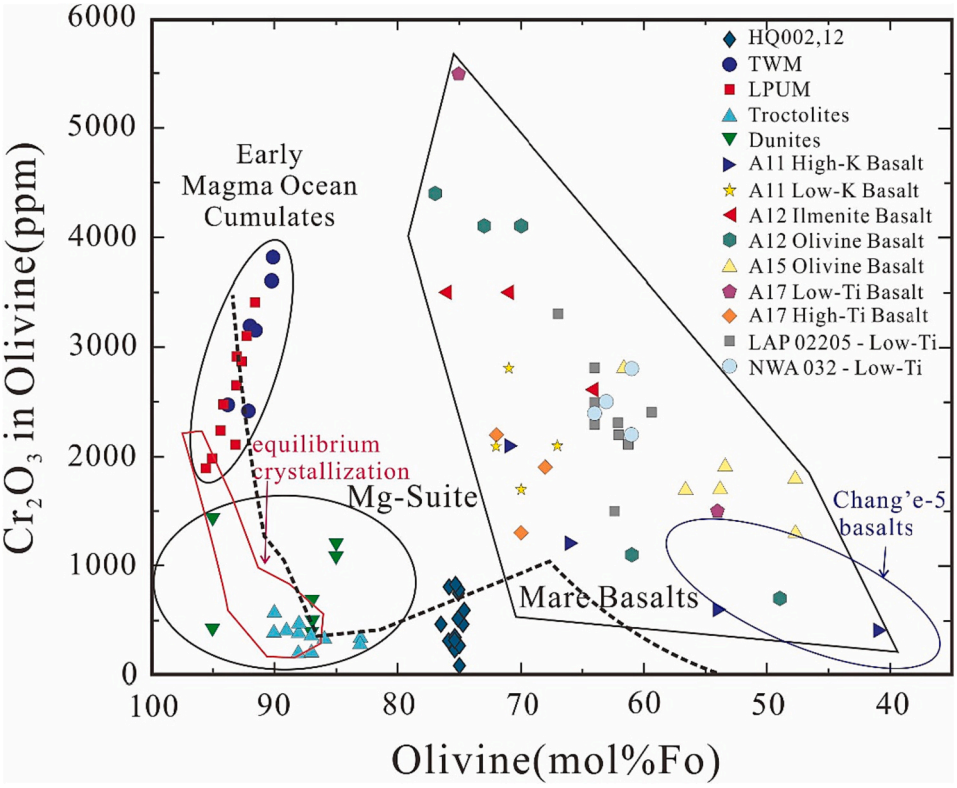

Fig. 7. The Cr_2O_3 concentrations versus Fo contents of olivine in different lunar materials. The figure was modified from Elardo et al. (2011). The black dashed line corresponds to our MELTS modeling fractional crystallization curve (calculated conditions: $P = 2$ kbar, fO_2: IW; starting composition melt B-1 from Ju et al., 2021). The olivine crystallized from melt formed through the decompression melting is from Ju et al. (2021) (red rectangular field-equilibrium crystallization). Early magma ocean cumulates experiment data from Elardo et al. (2011). Mg suite and mare basalt olivine data from Papike et al. (1998), Shearer and Papike (2005), and Elardo et al. (2011). Chang'e-5 basalts olivine data from He et al. (2022). TWM is the Taylor whole Moon, LPUM is lunar primitive upper mantle model. (For interpretation of the references to color in this figure legend, the reader is referred to the web version of this article.)

Table 2
Bulk Composition of magnesian granulite HQ002,12 (all in μg/g, except for major elements in wt%).

	HQ002 , 12	Chang'e-5 (Li et al., 2022)	NWA 10401		NWA 5744
(wt%)			IDRISI	XMapTools	
SiO_2	45.4 ± 0.32	42.2 ± 0.34	42.6	42.4	43.7
TiO_2	0.22 ± 0.00	5.00 ± 0.06	0.12	0.14	0.09
Al_2O_3	20.2 ± 0.12	10.8 ± 0.18	22.8	21.1	23.6
FeO	7.45 ± 0.14	22.5 ± 0.33	6.11	6.92	6.06
MnO	0.11 ± 0.00	0.28 ± 0.03	0.08	0.10	0.09
MgO	13.4 ± 0.28	6.48 ± 0.35	15.4	17.5	12.8
CaO	12.4 ± 0.09	11.0 ± 0.10	12.4	11.4	13.1
Na_2O	0.27 ± 0.00	0.26 ± 0.210	0.20	0.18	0.29
K_2O	0.01 ± 0.00	0.19 ± 0.15	b.d.	b.d.	–
P_2O_5	0.07 ± 0.00	0.23 ± 0.05	0.01	0.01	0.02
(ug/g)					
La	0.76 ± 0.03	36.1 ± 1.4	0.63	0.62	0.62
Ce	2.03 ± 0.05	92.8 ± 3.7	1.39	1.42	1.92
Pr	0.29 ± 0.02	12.5 ± 2.22	0.18	0.20	0.29
Nd	1.50 ± 0.08	–	0.88	0.98	1.49
Sm	0.49 ± 0.05	16.1 ± 0.60	0.28	0.32	0.52
Eu	0.53 ± 0.03	0.56 ± 0.10	0.56	0.56	0.47
Gd	0.69 ± 0.06	18.9 ± 0.77	0.26	0.36	0.70
Tb	0.13 ± 0.01	3.51 ± 0.28	0.04	0.06	0.13
Dy	0.85 ± 0.05	20.9 ± 1.4	0.34	0.47	0.90
Ho	0.19 ± 0.01	4.5 ± 1.4	0.07	0.10	0.19
Er	0.49 ± 0.03	–	0.21	0.29	0.59
Tm	0.07 ± 0.01	–	0.03	0.04	0.08
Yb	0.51 ± 0.04	–	0.25	0.30	0.57
Lu	0.08 ± 0.01	1.41 ± 0.08	0.04	0.05	0.08
Sc	11.05 ± 0.23	66 ± 2.6	–	–	n/a
Th	0.10 ± 0.01	4.72 ± 0.28	0.01	0.02	0.10
Sr	103.1 ± 0.74	–	n/a	n/a	n/a
Total	99.60	98.90	99.9	100.0	99.8

Abbreviation: n/a = not analyzed; b.d. = below detection limit.
Change-5 data from Li et al. (2022). NWA10401 data from Gross et al. (2020). NWA 5744 data from Kent et al. (2017).
IDRISI and Xmap Tools are two computational programs used to calculate modal mineralogy of the sample. The modal mineralogy obtained by the programs in conjunction with mineral chemistry was then used to calculate whole-rock bulk composition of the sample.

$0.0585 \times T + 39.233$ (Fig. S4). This equation has been used to predict the DCr^{Ol}_{melt} values for the temperatures along a liquid line of descent calculated using our MELTS approach.

Fig. 7 clearly illustrates (black dashed line) that the predicted olivine compositions align with the Mg-suite data, including samples from the Apollo mission (troctolites) and the troctolite clasts from our study. The calculated olivine compositions appear to be slightly shifted towards lower Fo numbers compared to the equilibrium crystallization model by Ju et al. (2021). This discrepancy, however, could potential be resolved through minor tweaking of the starting composition, oxygen fugacity, and/or crystallization pressure. Consequently, there is a plausible genetic connection between the Mg-suite rocks, and our troctolites, suggesting that the latter may be pristine and formed during a later stage along a fractional crystallization path. This scenario challenges the hybridization model and strengthens the evidence in favour of the fractional crystallization modeling.

The decompression melting model of Prissel and Gross (2020) in that Mg-suite source region is in line with the isotopic data that explain the age overlap between the Mg-suite and anorthosite (Borg et al., 2020). This onsistency implies that the Mg-suite source was either an undifferentiated component or a cumulate produced very early in LMO solidification. Meanwhile, that Mg-suite magmatism was occurring outside of PKT was supported by recent 3D dynamic simulations of mantle overturn (Prissel et al., 2023). The new mantle overturn models demonstrate that the lower lunar mantle (modeled as a peridotite source) experiences modest degrees of partial melting which can explain the key volume, geochronological, and spatial characteristics of Mg-suite magmatism (Prissel et al., 2023). In summary, the clast HQ002,12 studied here, support the decompression melting model of Prissel and Gross (2020) for the source of melt that subsequently may crystallized via fractional crystallization as our MELTS model suggests for a population of troctolites.

4.2. Proposed origin of the magnesian granulites

Shearer et al. (2015) showed that Mg-suite rocks can be produced by placing hot, less dense early magma ocean cumulates into the plagioclase-rich primordial crust, which would produce Mg-suite parent magmas. Thus, outside the PKT, Mg-suite magmas would not be required to have a KREEP signature (Korotev et al., 2003; Shearer et al., 2015). To date, no consensus has been reached on this topic, and it is unclear whether KREEP is a required component of Mg-suite magmatism or represents a secondary addition. If KREEP is concentrated inthe PKT, Mg-suite magmatism outside of the PKT region may not contain a significant large amount of KREEP component (e.g., (Lucey et al., 2000; Gross and Joy, 2016; Korotev et al., 2003; Prissel et al., 2015; Prissel et al., 2016a, 2016b).

Calzada-Diaz et al. (2015) developed a computational program that utilizes data from the Lunar Prospector Gamma-Ray Spectrometer (LP-GRS) to compare the composition of the lunar surface with whole-rock bulk compositions of lunar samples. This program was applied to investigate the potential source regions of granulitic meteorite NWA 10401 (Gross et al., 2020), where bulk Fe and Ti of NWA 10401 were used to match the composition of the lunar surface. The results indicate that the possible source regions of NWA 10401 were located in the lunar highlands, some of which were on the far side of the Moon (Fig. 8).

The unique lithology of HQ002,12 indicates that it did not originate from the local CE-5 basalts. It is hypothesized that the clast may have been originate from three possible sources: 1) excavation from the buried highland materials beneath the landing site by overlapping mare basalts, 2) transport from the adjacent highlands in the Procellarum-KREEP-Terrane, or 3) transport from the highlands outside the Procellarum-KREEP-Terrane, as proposed by Qian et al. (2021b). However, the low abundance of incompatible trace elements, including K, P, Th, U, and REE, in HQ002,12 largely deviates from the highland crustal materials in the Procellarum-KREEP-Terrane, as reported by Prettyman et al. (2006). Consequently, it is improbable that HQ002,12 was excavated from the underlying KREEP crust beneath the mare basalts.

In contrast, the lithology of HQ002,12 suggests that it may have been transported from its original source site through an impact process over a great distance outside the Procellarum-KREEP-Terrane, as reported by previous studies (Arvidson et al., 1975; Hörz et al., 1991; Xiao et al., 2013). Given the compositional similarities between HQ002,12 and NWA 10401 (see Figs. 3, 5; Table 2), it is inferred that HQ002,12 could have originated from a source similar to NWA 10401.

The stratigraphy of the Chang'e-5 landing site provides a solid basis for interpreting the context for the provenance of the samples collected from the lunar regolith. There are different layers in the CE-5 landing site, including impact ejecta, regolith, moderate-Ti basalts, paleo-ejecta, paleo-regolith, low-Ti mare basalts, and PKT crust, which can be tested by Lunar Penetrating Radar onboard CE-5(Qian et al., 2021c). The regolith is predicted to have a thickness of ~4–7 m at the CE-5 landing site. Underneath it is the Eratosthenian-aged mare basalts (Chang'e-5 Em4/P58 and Em3). Underlying Eratosthenian-aged basalts are paleo-ejecta and paleo-regolith layers, derived from the long exposure (~2 Ga) to the space environment of Imbrian-aged low-Ti mare basalts (Im2) after its emplacement, until being buried by the Eratosthenian-aged mare basalts. The composition of paleo-ejecta is likely to be dominated by the Pythagoras crater.

The most plausible source crater for the clast HQ002,12 is the Pythagoras crater located to the north of the CE-5 landing site (Fig. 8). With a diameter of approximately 145 km, the ejecta from Pythagoras crater could have been deposited between the Eratosthenian-aged and Imbrian-aged mare basalts beneath the CE-5 landing site with a

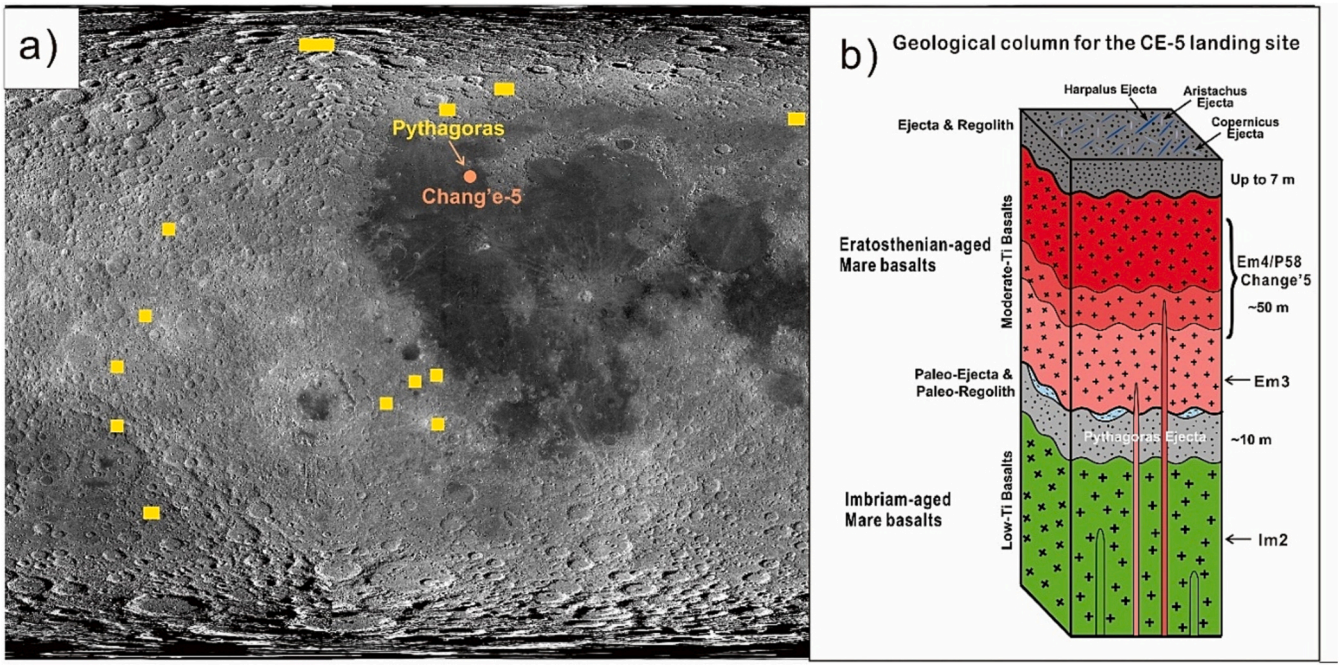

Fig. 8. Potential source craters of HQ002,12 and NWA 10401. a) The potential source craters are from Gross et al. (2020). b) The geological column for the CE-5 landing site, modified from Qian et al. (2021c). The most plausible source crater for the clast HQ002,12 is the Pythagoras crater located to the north of the CE-5 landing site. The paleo-ejecta from Pythagoras crater could have been deposited between the Eratosthenian-aged and Imbrian-aged mare basalts beneath the CE-5 landing site.

thickness of about 1.7 m, as noted by (Qian et al., 2021c). Pythagoras crater is also the closest potential source crater for NWA 10401, with its ejecta present beneath the CE-5 landing site, as reported by Qian et al. (2021c). Later impacts on the Eratosthenian-aged basalts may have excavated the underlying older materials, such as paleo-ejecta from Pythagoras crater, and delivered them to the CE-5 site (Qian et al., 2021b). As a result, HQ002,12 was most likely the product of multiple impacts on a source originally located >100 km away. Orbital observations also suggest Mg-suite locations outside of the PKT (e.g., Pieters et al., 2014; Sun et al., 2017). This illustrate an alternative mechanism (impact ejecta from outside the PKT) as a possible explanation for the presence of Mg-suite within the PKT.

4.3. *Impact that formed the clast HQ002,12*

The two-pyroxene thermometer proposed by Lindsley and Andersen (1983)has been commonly utilized to assess the metamorphic temperatures of lunar materials. This method has yielded equilibration temperatures between 940 and 1210 °C for both Apollo and lunar meteorite granulites, as reported in previous studies (Çushing et al., 1999; Hudgins, 2009; Kent et al., 2017). Lunar granulites are believed to have formed exclusively via thermal metamorphism at temperatures exceeding 1000 °C, which was adequate for complete re-equilibration of minerals.

The calculated cooling rates of the granulite suite have been used to provide insights into the crustal conditions under which they formed. Early investigations of two Apollo granoblastic samples (79,215,52 and 67,915,221; representative of the fine-grained granoblastic granulites) using crystal size distributions derived from photomicrographs suggested cooling rates ranging from 0.5 to 30 °C a^{-1} (Çushing et al., 1999). Further analysis of matrix pyroxenes in NWA 5744, with an average width of ~5 μm, indicated rapid cooling after metamorphism, possibly taking as little as 15–1500 years (Kent et al., 2017). Some finer-grained (<5 μm) granoblastic granulite clasts were estimated to have experienced much faster cooling rates, ranging from hundreds to thousands of degrees centigrade per year. Given these calculations, it is possible that the fine-grained HQ002,12 sample underwent metamorphism at or near the lunar surface, where rapid heat dissipation could have accommodated such short durations.

Pernet-Fisher and Joy (2021) provided a comprehensive summary of the possible environments in which granulites could have originated, and the origin of the metamorphic heat source has been used to infer the locations within the lunar crust where metamorphism may have occurred. Based on this, two possible locations have been proposed. The first is near-surface locations resulting from the burial of the uppermost (<10 km) crustal rocks by impact melt sheets or hot fall-back breccias, as described previously (Çushing et al., 1999; Hudgins et al., 2011). The second is in deep crustal (>10 km) locations resulting from contact metamorphism due to the emplacement of magma chambers/plutons, as described in Wieczorek et al. (2006). In this context, the HQ002,12 could possibly represent a lithology above an impact melt sheet (such as fall-back ejecta), which would imply the need for large impactors (>100 km) to generate such thick melt sheets.

Obtaining mineral separates from fine-grained rocks such as HQ002,12 for robust internal isochron calculations using Rb—Sr or Sm—Nd isotope chronometer systems is challenging (Papike et al., 1998; McLeod et al., 2016). The protoliths of the granulite suite likely represent lunar highland lithologies that have undergone modification by impacts. Mg-suite rocks exhibit overlapping ages of approximately 4.34 Ga, which is similar to the average age of the mare basalts mantle source region and the model age for urKREEP (Borg et al., 2020). Several studies have utilized multiple chronometers on granulite NWA 3163 to constrain a protolith age >4.3 Ga (White et al., 2020); McLeod et al., 2016). The reported metamorphic ages of meteorites are younger than those of Apollo granulites; for instance, the granulitic meteorites NWA 3163, NWA 4881, and Dhofar 026 have ages <3.8 Ga (McLeod et al., 2016).

The Chang'e-5 mission of China successfully returned lunar soils from the Em4/P58 mare plain located in the Northern Oceanus Procellarum, which revealed the youngest dated lunar mare basalts to date at ~2.0 Ga (Li et al., 2021; Che et al., 2021). The clast HQ002,12 was discovered within the CE-5 lunar soil, indicating a rather young impact

age (< 2.0 Ga) that may be associated with a recent and isolated impact event, leading to the transport of the clast to the CE-5 landing site.

5. Conclusions

Two magnesian troctolitic granulites with granoblastic texture have been discovered in the CE-5 lunar soil, representing components likely derived from impact craters in adjacent highlands that excavated the materials and transported them to the landing site. One of the clasts, HQ002,12, is composed of two lithologies, anorthosite and a magnesian-rich lithology namely Mg troctolitic granulite. The troctolitic granulite has granoblastic texture, consisting of plagioclase (64.6 vol%), olivine (23.7 vol%), pyroxene (11.6 vol%), and traces of chromite and troilite (<0.1 vol%). Olivine in the troctolitic granulite has a composition in the range $Fo_{74.7–76.5}$, slightly lower than the values reported for the Mg granulites NWA 5744 and NWA 1040, but higher than those given in Fe-granulites (e.g., NWA 3163). The bulk Mg# (76) is also slightly lower than the one reported for the NWA 5744 and NWA 10401. The trace element content shows low incompatible element abundance and negligible KREEP content (KREEP-poor), similar to NWA 5744 and NWA 10401. The presence of chromite and the low Cr content in olivine imply that the protolith of HQ002,12 may suggests a plausible genetic connection between the Mg-suite rocks, and our troctolites, suggesting that the latter may be pristine and formed during a later stage along a fractional crystallization path. This scenario challenges the hybridization model and strengthens the evidence in favour of the fractional crystallization modeling.

The Pythagoras crater to the north of the CE-5 landing site is the most plausible source for the ejecta that deposited between the Eratosthenian-aged and Imbrian-aged mare basalts under the CE-5 site. A subsequent impact on the Eratosthenian-aged basalts may excavated the underlaying older materials such as the paleo-ejecta from Pythagoras crater and delivered them to the CE-5 site. The metamorphism of HQ002,12 likely resulted from shallow burial of the uppermost crustal rocks (<10 km) due to impact.

Supplementary data to this article can be found online at https://doi.org/10.1016/j.icarus.2023.115853.

Declaration of Competing Interest

The authors declare no conflict of interest.

Data availability

Data will be made available on request.

Acknowledgments

We cordially thank China National Space Administration (CNSA) for supporting the Chang'e-5 mission and providing access to the CE-5 sample CE5Z0204YJFM002. Many thanks to Tabb C. Prissel and Randy L. Korotev for their thoughtful comments on this manuscript. This research is funded by the Pre-Research Project on Civil Aerospace Technologies (D020205, D020101) and China University of Geosciences (CUG) outstanding youth team project (G1323523042).

References

Arvidson, R., et al., 1975. Horizontal transport of the regolith, modification of features, and erosion rates on the lunar surface. Moon 13, 67–79.
Asimow, P.D., 1999. A model that reconciles major-and trace-element data from abyssal peridotites. Earth Planet. Sci. Lett. 169 (3–4), 303–319.
Asimow, P.D., Ghiorso, M.S., 1998. Algorithmic modifications extending MELTS to calculate subsolidus phase relations. Am. Mineral. 83 (9–10), 1127–1132.
Asimow, P.D., Hirschmann, M.M., Stolper, E.M., 2001. Calculation of peridotite partial melting from thermodynamic models of minerals and melts, IV. Adiabatic decompression and the composition and mean properties of mid-ocean ridge basalts. J. Petrol. 42 (5), 963–998.
Asimow, P.D., Dixon, J.E., Langmuir, C.H., 2004. A hydrous melting and fractionation model for mid-ocean ridge basalts: application to the mid-Atlantic ridge near the Azores. Geochem. Geophys. Geosyst. 5 (1).
Bence, A.E., Papike, J.J., 1972. Pyroxenes as recorders of lunar basalt petrogenesis: chemical trends due to crystal-liquid interaction. In: Lunar and Planetary Science Conference Proceedings, vol. 3, p. 431.
Bickel, Ch.E., Warner, J.L., 1978. Survey of lunar plutonic and granulitic lithic fragments. In: Lunar and Planetary Science Conference Proceedings, pp. 629–652.
Borg, Lars E., et al., 2020. The formation and evolution of the Moon's crust inferred from the Sm-Nd isotopic systematics of highlands rocks. Geochim. Cosmochim. Acta 290, 312–332.
Calzada-Diaz, A., et al., 2015. Constraining the source regions of lunar meteorites using orbital geochemical data. Meteorit. Planet. Sci. 50, 214–228.
Cao, Haijun, et al., 2022. A Raman spectroscopic and microimage analysis perspective of the Chang'e-5 lunar samples. Geophys. Res. Lett. 49.
Che, Xiaochao, et al., 2021. Age and composition of young basalts on the moon, measured from samples returned by Chang'e-5. Science 374, 887–890.
Çushing, Janet A., et al., 1999. The granulitic impactite suite: impact melts and metamorphic breccias of the early lunar crust. Meteorit. Planet. Sci. 34, 185–195.
Day, J.M., Floss, C., Taylor, L.A., Anand, M., Patchen, A.D., 2006. Evolved mare basalt magmatism, high Mg/Fe feldspathic crust, chondritic impactors, and the petrogenesis of Antarctic lunar breccia meteorites Meteorite Hills 01210 and Pecora escarpment 02007. Geochim. Cosmochim. Acta 70 (24), 5957–5989.
Dowty, Eric, et al., 1974. Ferroan anorthosite: A widespread and distinctive lunar rock type. Earth Planet. Sci. Lett. 24, 15–25.
Elardo, S.M., Draper, D.S., Shearer Jr., C.K., 2011. Lunar Magma Ocean crystallization revisited: bulk composition, early cumulate mineralogy, and the source regions of the highlands Mg-suite. Geochim. Cosmochim. Acta 75 (11), 3024–3045.
Floss, Christine, et al., 1998. Lunar ferroan anorthosite petrogenesis: clues from trace element distributions in FAN subgroups. Geochim. Cosmochim. Acta 62, 1255–1283.
Ghiorso, M.S., Sack, R.O., 1995. Chemical mass transfer in magmatic processes IV. A revised and internally consistent thermodynamic model for the interpolation and extrapolation of liquid-solid equilibria in magmatic systems at elevated temperatures and pressures. Contrib. Mineral. Petrol. 119, 197–212.
Goodrich, C.A., Taylor, G.J., Keil, K., Boynton, W.V., Hill, D.H., 1984. Petrology and chemistry of hyperferroan anorthosites and other clasts from lunar meteorite ALHA81005. J. Geophys. Res. Solid Earth 89 (S01), C87–C94.
Gross, Juliane, Joy, Katherine H., 2016. Evolution, lunar: From magma ocean to crust formation. In: Encyclopedia of Lunar Science.
Gross, J., Treiman, A.H., Mercer, C.N., 2014. Lunar feldspathic meteorites: constraints on the geology of the lunar highlands, and the origin of the lunar crust. Earth Planet. Sci. Lett. 388, 318–328.
Gross, Juliane, et al., 2020. Geochemistry and Petrogenesis of Northwest Africa 10401: a new type of the Mg-suite rocks. J. Geophys. Res.: Planets 125.
Haskin, Larry A., et al., 1998. The case for an Imbrium origin of the Apollo thorium-rich impact-melt breccias. Meteorit. Planet. Sci. 33, 959–975.
He, Q., et al., 2022. Detailed petrogenesis of the unsampled Oceanus Procellarum: the case of the Chang'e-5 mare basalts. Icarus 383.
Hörz, Friedrich, et al., 1991. 'Lunar surface processes. In: Lunar sourcebook.
Hu, Zhaochu, et al., 2008. Signal enhancement in laser ablation ICP-MS by addition of nitrogen in the central channel gas. J. Anal. At. Spectrom. 23.
Hudgins, Jillian Amy, 2009. Mineralogy, Petrology, and Chronology of the Lunar Granulitic Breccias. Japan Association for Earthquake Engineering.
Hudgins, Jillian A., et al., 2008. A laser probe 40Ar/39Ar and INAA investigation of four Apollo granulitic breccias. Geochim. Cosmochim. Acta 72, 5781–5798.
Hudgins, Jillian A., et al., 2011. Mineralogy, geochemistry, and 40Ar–39Ar geochronology of lunar granulitic breccia Northwest Africa 3163 and paired stones: comparisons with Apollo samples. Geochim. Cosmochim. Acta 75, 2865–2881.
Jochum, Klaus Peter, et al., 2005. GeoReM: a new geochemical database for reference materials and isotopic standards. Geostand. Geoanal. Res. 29, 333–338.
Jolliff, Bradley L., et al., 1996. Lithologic distribution and geologic history of the Apollo 17 site: the record in soils and small rock particles from the highland massifs. Meteorit. Planet. Sci. 31, 116–145.
Joy, K.H., Crawford, I.A., Russell, S.S., Kearsley, A.T., 2010. Lunar meteorite regolith breccias: an in situ study of impact melt composition using LA-ICP-MS with implications for the composition of the lunar crust. Meteorit. Planet. Sci. 45 (6), 917–946.
Ju, D.Y., Du, W., Li, R., Pang, R.L., 2021. Constraints on the source of the Lunar Mg-suite by thermodynamic simulation. Bull. Mineral. Petrol. Geochem. 40 (5), 1154–1165. https://doi.org/10.19658/j. issn.1007-2802.2021.40.078.
Kent, Jeremy J., et al., 2017. Mineralogy and petrogenesis of lunar magnesian granulitic meteorite Northwest Africa 5744. Meteorit. Planet. Sci. 52, 1916–1940.
Korotev, R.L., 2012. Lunar meteorites from Oman. Meteorit. Planet. Sci. 47 (8), 1365–1402.
Korotev, R.L., Irving, A.J., 2016. Not quite keeping up with the lunar meteorites—2016. In: 47th annual Lunar and Planetary Science Conference, p. 1358.
Korotev, Randy L., et al., 2003. Feldspathic lunar meteorites and their implications for compositional remote sensing of the lunar surface and the composition of the lunar crust. Geochim. Cosmochim. Acta 67, 4895–4923.
Li, C.L., et al., 2022. Characteristics of the lunar samples returned by the Chang'E-5 mission. Natl. Sci. Rev. 9.
Li, Q.L., et al., 2021. Two-billion-year-old volcanism on the moon from Chang'e-5 basalts. Nature 600, 54–58.
Lindsley, Donald H., Andersen, David J., 1983. A two-pyroxene thermometer. J. Geophys. Res. 88.

Lindstrom, Marilyn M., Lindstrom, David J., 1986. Lunar granulites and their precursor anorthositic norites of the early lunar crust. J. Geophys. Res. 91, 263–276.
Liu, Yongsheng, et al., 2008. In situ analysis of major and trace elements of anhydrous minerals by LA-ICP-MS without applying an internal standard. Chem. Geol. 257, 34–43.
Longhi, J., Walker, D., Hays, J.F., 1978. The distribution of Fe and Mg between olivine and lunar basaltic liquids. Geochim. Cosmochim. Acta 42 (10), 1545–1558.
Lucey, Paul G., et al., 2000. Imaging of lunar surface maturity. J. Geophys. Res.: Planets 105, 20377–20386.
Ma, M.-S., Schmitt, R.A., 1982. Chemistry of the matrix, the glass coating and an olivine clast from polymict ANT breccia 60035. In: Lunar and Planetary Science Conference, pp. 453–454.
McCallum, I.S., Schwartz, J.M., 2001. Lunar mg suite: Thermobarometry and petrogenesis of parental magmas. J. Geophys. Res.: Planets 106, 27969–27983.
McDonough, W.F., Sun, S.S., 1995. The composition of the earth. Chem. Geol. 120, 223–253.
McLeod, Claire L., et al., 2016. Constraints on formation and evolution of the lunar crust from feldspathic granulitic breccias NWA 3163 and 4881. Geochim. Cosmochim. Acta 187, 350–374.
Morse, Stearns Anthony, 1980. Basalts and Phase Diagrams: An Introduction to the Quantitative Use of Phase Diagrams in Igneous Petrology. Springer.
Pang, Runlian, et al., 2022. New occurrence of Seifertite and Stishovite in Chang'E-5 regolith. Geophys. Res. Lett. 49.
Papike, J.J., et al., 1996. Ion microprobe investigation of plagioclase and orthopyroxene from lunar mg-suite norites: implications for calculating parental melt REE concentrations and for assessing postcrystallization REE redistribution. Geochim. Cosmochim. Acta 60, 3967–3978.
Papike, J.J., et al., 1997. Evolution of the lunar crust: SIMS study of plagioclase from ferroan anorthosites. Geochim. Cosmochim. Acta 61, 2343–2350.
Papike, James J., et al., 1998. 'Lunar samples. In: Planetary materials (De Gruyter).
Pernet-Fisher, John F., Joy, Katherine H., 2021. Thermal metamorphism on the moon as recorded by the granulite suite. J. Geol. Soc. Lond. 179.
Pieters, C.M., et al., 2014. The distribution of Mg-spinels across the moon and constraints on crustal origin. Am. Mineral. 99, 1893–1910.
Prettyman, T.H., et al., 2006. Elemental composition of the lunar surface: analysis of gamma ray spectroscopy data from Lunar prospector. J. Geophys. Res.: Planets 111, n/a–n/a.
Prissel, Tabb C., Gross, Juliane, 2020. On the petrogenesis of lunar troctolites: new insights into cumulate mantle overturn & mantle exposures in impact basins. Earth Planet. Sci. Lett. 551.
Prissel, T.C., et al., 2015. Buoyancy driven magmatic ascent of Mg-suite parental melts. In: 46th Annual Lunar and Planetary Science Conference, p. 1158.
Prissel, Tabb C., et al., 2016a. Formation of the lunar highlands mg-suite as told by spinel. Am. Mineral. 101, 1624–1635.
Prissel, Tabb C., et al., 2016b. On the potential for lunar highlands Mg-suite extrusive volcanism and implications concerning crustal evolution. Icarus 277, 319–329.
Prissel, T.C., Zhang, N., Jackson, C.R.M., Li, H., 2023. Rapid transition from primary to secondary crust building on the moon explained by mantle overturn. Nat. Commun. 14, 5002. https://doi.org/10.1038/s41467-023-40751-7.
Qian, Y., et al., 2021a. Young lunar mare basalts in the Chang'e-5 sample return region, northern Oceanus Procellarum. Earth Planet. Sci. Lett. 555.
Qian, Y., Xiao, L., Head, J.W., Wöhler, C., Bugiolacchi, R., Wilhelm, T., Althoff, S., Ye, B., He, Q., Yuan, Y., Zhao, S., 2021b. Copernican-aged (<200 Ma) impact ejecta at the Chang'e-5 landing site: statistical evidence from crater morphology, morphometry, and degradation models. Geophys. Res. Lett. 48 (20) https://doi.org/10.1029/2021GL095341 e2021GL095341.
Qian, Y., Xiao, L., Wang, Q., Head, J.W., Yang, R., Kang, Y., van der Bogert, C.H., Hiesinger, H., Lai, X., Wang, G., Pang, Y., Zhang, N., Yuan, Y., He, Q., Huang, J., Zhao, J., Wang, J., Zhao, S., 2021c. China's Chang'e-5 landing site: geology, stratigraphy, and provenance of materials. Earth Planet. Sci. Lett. 561, 116855 https://doi.org/10.1016/j.epsl.2021.116855.
Salpas, P.A., Lindstrom, M.M., Taylor, L.A., 1988. Highland materials at Apollo 17-Contributions from 72275. In: Lunar and Planetary Science Conference Proceedings, vol. 18, pp. 11–19.
Shearer, C.K., Hess, P.C., Wieczorek, M.A., et al., 2006. Thermal and magmatic evolution of the Moon. Rev. Mineral. Geochem. 60, 365–518.
Shearer, Charles K., Papike, J.J., 2005. Early crustal building processes on the moon: Models for the petrogenesis of the magnesian suite. Geochim. Cosmochim. Acta 69, 3445–3461.
Shearer, C.K., Elardo, S.M., Petro, N.E., Borg, L.E., McCubbin, F.M., 2015. Origin of the lunar highlands Mg-suite: an integrated petrology, geochemistry, chronology, and remote sensing perspective. Am. Mineral. 100 (1), 294–325.
Sheng, Si-Zhang, et al., 2022. First location and characterization of Lunar Highland clasts in Chang'E 5 Breccias using TIMA-SEM-EPMA. At. Spectrosc. 43, 352–363.
Shervais, John W., McGee, James J., 1998. Ion and electron microprobe study of troctolites, norite, and anorthosites from Apollo 14: evidence for urKREEP assimilation during petrogenesis of Apollo 14 Mg-suite rocks. Geochim. Cosmochim. Acta 62, 3009–3023.
Smith, P.M., Asimow, P.D., 2005. Adiabat_1ph: A new public front-end to the MELTS, pMELTS, and pHMELTS models. Geochem. Geophys. Geosyst. 6 (2).
Stoffler, D., 2006. Cratering history and Lunar chronology. Rev. Mineral. Geochem. 60, 519–596.
Stöffler, D., et al., 1980. Recommended classification and nomenclature of lunar highland rocks-a committee report. In: Lunar Highlands Crust, pp. 51–70.
Stöffler, D., Hamann, C., Metzler, K., 2018. Shock metamorphism of planetary silicate rocks and sediments: proposal for an updated classification system. Meteorit. Planet. Sci. 53 (1), 5–49.
Sun, Y., Li, L., Zhang, Y., 2017. Detection of Mg-spinel bearing central peaks using M3 images: Implications for the petrogenesis of Mg-spinel. Earth Planet. Sci. Lett. 465, 48–58.
Takeda, Hiroshi, et al., 2006. Magnesian anorthosites and a deep crustal rock from the farside crust of the moon. Earth Planet. Sci. Lett. 247, 171–184.
Tian, H.C., et al., 2021. Non-KREEP origin for Chang'e-5 basalts in the Procellarum KREEP terrane. Nature 600, 59–63.
Treiman, Allan H., et al., 2010. Magnesian anorthositic granulites in lunar meteorites Allan Hills A81005 and Dhofar 309: geochemistry and global significance. Meteorit. Planet. Sci. 45, 163–180.
Warren, Paul H., 1993. A concise compilation of petrologic information on possibly pristine nonmare moon rocks. Am. Mineral. 78, 360–376.
White, L.F., et al., 2020. Evidence of extensive lunar crust formation in impact melt sheets 4,330 Myr ago. Nat. Astron. 4, 974–978.
Wieczorek, M.A., et al., 2006. The constitution and structure of the Lunar interior. Rev. Mineral. Geochem. 60, 221–364.
Xiao, Zhiyong, et al., 2013. Mass wasting features on the moon – how active is the lunar surface? Earth Planet. Sci. Lett. 376, 1–11.
Xu, Xiaoqing, Hui, Hejiu, Chen, Wei, Huang, Shichun, Neal, Clive R., Xu, Xisheng, 2020. Formation of lunar highlands anorthosites. Earth Planet. Sci. Lett. 536, 116138.
Yamaguchi, A., et al., 2010. The variety of lithologies in the Yamato-86032 lunar meteorite: implications for formation processes of the lunar crust. Geochim. Cosmochim. Acta 74, 4507–4530.
Zeng, X., Li, X., Liu, J., et al., 2023. Exotic clasts in Chang'e-5 regolith indicative of unexplored terrane on the moon. Nat. Astron. 7, 152–159. https://doi.org/10.1038/s41550-022-01840-7.